Neutron Total Cross Sections in the 7- to 14-Mev Region*

A. BRATENAHL, J. M. PETERSON, AND J. P. STOERING
University of California Radiation Laboratory, Livermore, California

(January 29, 1958)

The neutron total cross sections for 35 elements and isotopes were measured at several energies between 7 and 14 Mev using monoenergetic neutrons produced by the Livermore variable-energy cyclotron through the $D(d,n)He^3$ reaction. The effects of beam contamination by gamma rays and low-energy "breakup" neutrons were evaluated through time-of-flight measurements and were kept small by suitably high bias on the plastic scintillator detector. The accuracy of the cross sections is typically ± 1 to 2%. Where comparisons with previous data are possible, the agreement ranges from excellent to poor (10% discrepancy). The data form a smooth cross-section surface when plotted *versus* energy and mass number, as expected on the basis of the optical model. The functional dependence on energy and mass is not simple but is in good agreement with the predictions of the optical model of Bjorklund and Fernbach.

I. INTRODUCTION

A SERIES of neutron total cross-section measurements has been undertaken to extend the range of experimental data up to neutron energies of about 30 Mev. Similar data in the 1- to 3-Mev energy range[1] helped stimulate the development of the optical model of the nucleus.[2,3] Since the real and imaginary potentials and the spin-orbit terms of this model are energy-dependent, it was felt that more extensive data on the energy dependence of the total cross sections would help evaluate the model.[4]

Probably the most accurate of the existing total cross-section data in the medium-energy range were produced by Coon, Graves, and Barschall[5] on an extensive series of elements using a pure 14-Mev neutron source. Nereson and Darden[6,7] measured a series of elements over the energy range of 3 to 13 Mev using a difficult technique involving the tail of the neutron spectrum from a fast reactor; the tie-in of their data with other data at 3 Mev (largely that of the Wisconsin group[8,9]) is good, but the tie-in with the data of Coon *et al.* at 14 Mev is only fair. Because of their fast-falling neutron energy spectrum (a factor of 10 drop every 3 Mev), the accuracy of the Nereson and Darden data inherently decreased in the high end of their range.

In addition to these extensive sets of data, a few other smaller sets of data exist, each covering fewer elements and a small energy interval in the range of 5 to 25 Mev. These can best be reviewed by referring to the neutron cross-section compilation BNL-325 (and its Supplement I),[10] plus the recent work of Bondelid *et al.*[11] and of Conner.[12]

This survey of the existing data made it seem worthwhile to measure the total cross sections of an extensive series of elements up to 30 Mev and down to a point where there is a comfortable overlap with the existing data. The variable-energy cyclotron in Livermore is capable of producing fairly monoenergetic neutrons up to about 30 Mev, which set the upper limit of the energy range. This paper is a report on the work in the energy range from 7 to 14 Mev. The work in the higher energy range has started and will be reported as soon as possible.

II. APPARATUS

The experiment consists of measuring the transmission of monoenergetic neutrons in good geometry, the usual method of measuring total cross sections. The neutrons are produced by $d-d$ reactions using the deuteron beam from the 90-inch variable-energy cyclotron. Beyond the cyclotron the main parts of the experimental setup (Fig. 1) are the deuterium gas target, the neutron collimator, the samples, and the detector.

The gas target consists of a cylindrical stainless steel housing $1\frac{1}{2}$ inches in diameter and 4 inches in length filled with deuterium gas at a pressure of slightly more than one atmosphere. Deuterons enter the target through a tantalum foil $1\frac{1}{4}$ inch in diameter and typically 34 mg cm^{-2} in thickness; the position of the incident deuteron beam is defined 10 inches in front of the target by a tantalum collimator $\frac{3}{4}$ inch in diameter.

The neutron collimator selects neutrons coming along a horizontal line from the gas target. (The deuteron beam is inclined 3.5 degrees from horizontal.) The collimator consists of a conical hole in a 2-ft block of iron, which allows a neutron cone of about 2.7 inches in radius at the sample position. The apex (projected) of

* This work was performed under the auspices of the U. S. Atomic Energy Commission.

[1] H. H. Barschall, Phys. Rev. **86**, 431 (1952).
[2] Fernbach, Serber, and Taylor, Phys. Rev. **75**, 1352 (1949).
[3] V. F. Weisskopf, Phys. Rev. **86**, 582(T) (1952); Feshbach, Porter, and Weisskopf, Phys. Rev. **90**, 166 (1953).
[4] F. E. Bjorklund and S. Fernbach, Phys. Rev. **109**, 1295 (1958).
[5] Coon, Graves, and Barschall, Phys. Rev. **88**, 562 (1952).
[6] N. Nereson and S. Darden, Phys. Rev. **89**, 775 (1953).
[7] N. Nereson and S. Darden, Phys. Rev. **94**, 1678 (1954).
[8] Miller, Adair, Bockelman, and Darden, Phys. Rev. **88**, 83 (1952).
[9] Walt, Becker, Okazaki, and Fields, Phys. Rev. **89**, 1271 (1953).
[10] *Neutron Cross Sections*, compiled by D. J. Hughes and J. A. Harvey, Brookhaven National Laboratory Report BNL-325 (Superintendent of Documents, U. S. Government Printing Office, Washington, D. C., 1955), Supplement I, 1957.
[11] Bondelid, Dunning, and Talbott, Phys. Rev. **105**, 193 (1957).
[12] J. P. Conner, Bull. Am. Phys. Soc. Ser. II, **2**, 267 (1957).

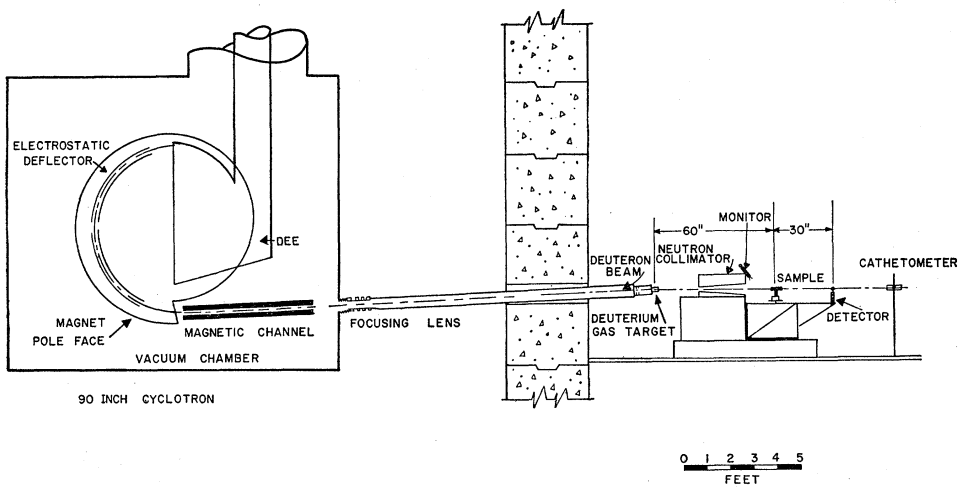

FIG. 1. Total cross section experimental arrangement. Elevation view.

the conical hole lies in front of the gas target, so that the inside surface of the collimating hole is not illuminated by the direct neutron beam. The iron block is imbedded in a large mass of concrete (3×4×4 ft), which serves to prevent inscattering from neighboring samples and sample supports and to reduce the general background. The experiment testing the effectiveness of this shielding assembly showed that the concrete block and collimator reduce background by a factor of 3.

The samples are in most cases cylinders having a diameter of 1 inch and a length of about 2 mean free paths. The copper sample used in the determination of background is also 1 inch in diameter and approximately 12 mean free paths long. The majority of the scattering materials are of the highest purity available, in most cases 99.9% or better. Impurities were checked by quantitative chemical analysis, and the possible existence of cavities in the materials was determined by radiographing each sample. In the fabrication of most of the samples, the materials were obtained oversized and then machined to insure uniform diameter and parallel ends.

The positioning of the samples is accomplished by means of an aluminum cart moving perpendicular to the neutron beam on a track mounted on a "power-strut" framework. The cart carries ten vertical Bakelite tubes, which support the individual samples. The cart, track, and tubes are independently adjustable, enabling a simple alignment procedure for all the samples placed on the cart. A separation of approximately 4 inches between samples insures that the adjacent positions are entirely free of the collimated neutron cone. The same "power-strut" structure supplies rigid support for the detector photomultiplier and preamplifier, thus eliminating any relative disturbance between the sample and the detector. The cart is driven by a continuous chain coupled by a simple gear train to a Selsyn motor and mechanical register and is remotely operated through another Selsyn in the control room. The sample position is known from the indication of a second register geared to the control Selsyn.

Alignment of the samples is achieved by placing a cathetometer approximately 10 feet behind the detector along a horizontal line through the center of the target. Along this line of sight, both ends of the collimator, each sample, and the detector are carefully aligned. Following the alignment of an individual sample, its corresponding register reading is recorded and later optically rechecked several times for reproducibility of position. A sample can be remotely set to within 0.008 inch. Backlash in the chain, gears, and Selsyn are negligible. A study of the change in transmission as the sample eclipses the detector shows that a misalignment of at least $\frac{1}{8}$ inch in the sample is necessary to increase the transmission by 1%.

The detector is a $\frac{1}{2}$-inch-diameter plastic scintillator coupled to an RCA 6199 photomultiplier tube by means of a 3-inch tapered light pipe. Gain drifts in the photomultiplier and preamplifier due to changes in temperature are minimized by a water-cooling method described by Ball, Booth, and MacGregor.[13] The remainder of the electronics is essentially the same as that used by Ball *et al.*[14] Output signals from the preamplifier are fed into an amplifier (linear to within 1% in the voltage range of the experiment), the output of which is fed to 5 discriminator-scalers.

The neutron beam is monitored by a counter identical to the detector. The monitor is located directly above the exit end of the collimator.

III. EXPERIMENTAL PROCEDURE

At the beginning of a set of runs of a given energy, the first step is the selection of the appropriate bias settings for the detector and monitor. The basis of this selection is the shape of the recoil-proton pulse-height spectrum from the plastic scintillators. Typically this spectrum (Fig. 2) is nearly flat in its upper half but diverges

[13] Ball, Booth, and MacGregor, Nuclear Instr. **1**, 71 (1957).
[14] Ball, Booth, and MacGregor, University of California Radiation Laboratory Report UCRL-4790, 1956 (unpublished).

rapidly in the lower half because of the large number of gamma-ray and low-energy-neutron signals. The low-energy-neutron contamination arises mainly from $d(d,pn)d$ and $d(d,2np)p$ breakup in the gas target. The lowest bias must not be so low that a significant contribution of gamma rays and low-energy neutrons is passed. It is found that setting the low bias at the point where the pulse-height spectrum begins to depart from flatness is adequate. This is shown by an auxiliary experiment in which the detected signals from gamma rays, from low-energy neutrons, and from the monoenergetic neutrons are differentiated by time-of-flight and their relative strengths measured as a function of bias. Figure 3 shows the time spectrum of detected particles in the nominal 14-Mev neutron beam for two bias settings. From time spectra such as these the curves in Fig. 4 are constructed, showing the effective gamma and low-energy-neutron contamination per detected "good"

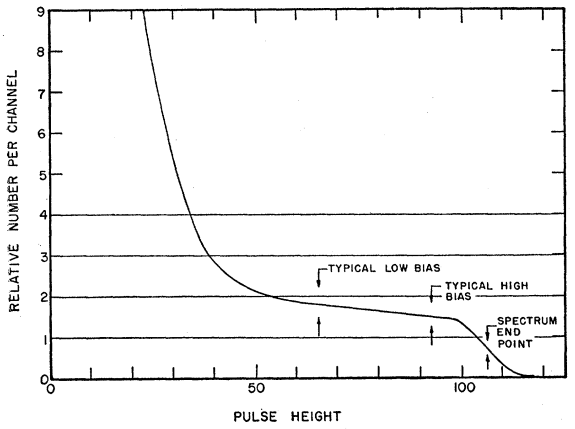

FIG. 2. The differential pulse-height spectrum from the ½-in. diameter plastic scintillator detector exposed to the nominal 14-Mev neutron beam.

neutron as a function of the fractional bias (ratio of the bias to the maximum good-neutron pulse height). At the chosen bias the unwanted contribution in most cases is less than 0.5% of the primary signal. The beam contaminants can either increase or decrease the measured cross section, depending on whether their cross sections are greater or smaller than that of the primary beam. The amount of error depends also upon the length of the sample. For example, a 1% 1-Mev gamma contaminant in a 14-Mev neutron beam will cause a 1.3% error in a 50% transmission lead sample but only a 0.5% error in a 2-mean-free-path sample. On the other hand, among the very light elements, where neutrons attenuate faster than gamma rays, the shorter the sample the better in this respect. In most of our cases the errors due to contaminants are negligible, but in the cases of hydrogen, lithium, and beryllium at the lower energies we have possible systematic errors of the order of -0.5 to -1.0% due to gamma contaminants.

As another check of the experimental method, curves

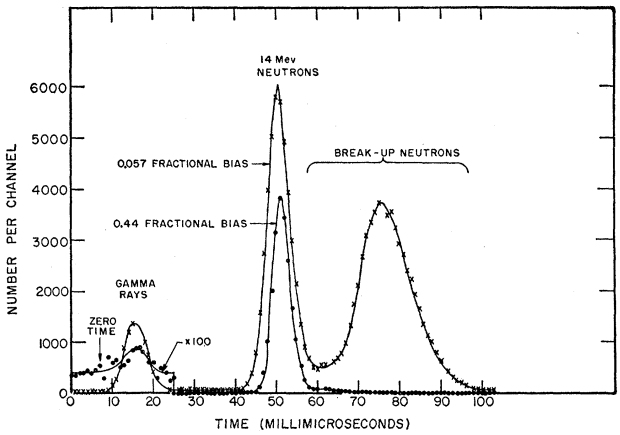

FIG. 3. Time-of-flight spectra of the nominal 14-Mev neutron beam as seen by the ½-in. diameter scintillator detector with two discriminator settings.

of transmission *vs* sample length were run on copper and lead at 14 Mev. These curves were straight line exponentials as far as they could be followed (more than two decades), but this method is not as sensitive as the time-of-flight method for detecting beam contaminants.

Three discriminator scalers are set at the low bias, and two others at a bias just below the upper end of the

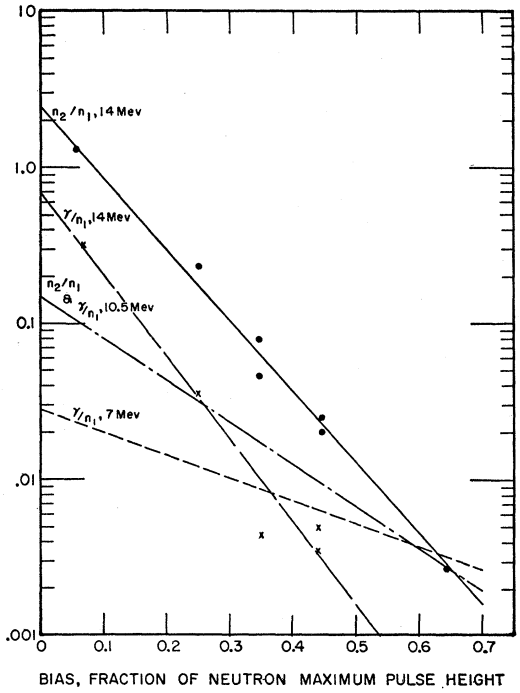

FIG. 4. Amount of gamma-ray and low-energy neutron beam contaminants relative to the number of detected "good" neutrons from the $d-d$ reaction as a function of the relative bias on the ½-inch-diameter plastic scintillator. These are shown for the nominal 7-, 10.5-, and 14-Mev neutron beams. For the 7-Mev neutron beam there was no measurable low-energy neutron contaminant; the deuteron beam energy here is below threshold for the $d-d$ breakup reaction.

TABLE I. Total cross sections in the 7- to 14-Mev range.

Element	E_n Mev	σ_t barns	E_n Mev	σ_t barns	E_n Mev	σ_t barns	E_n Mev	σ_t barns	E_n Mev	σ_t barns
H	7.17	1.24±0.02	8.77	1.04±0.01	10.42	0.94±0.02	13.13	0.76±0.02	14.02	0.72±0.01
H					11.13	0.88±0.02				
D	7.17	1.32±0.02	8.77	1.12±0.01	11.13	1.02±0.02	13.13	0.88±0.02	14.01	0.86±0.02
Li^6	7.01	1.92±0.02	8.54	1.75±0.03	11.18	1.65±0.02	12.63	1.53±0.02	13.98	1.45±0.02
Li^7	7.01	2.02±0.02	8.54	1.81±0.02	11.18	1.64±0.02	12.63	1.55±0.02	13.99	1.50±0.02
Be	6.83	1.75±0.02	8.57	1.68±0.02	10.24	1.66±0.02	12.63	1.56±0.01	14.11	1.51±0.02
C	7.12	0.79±0.01	8.77	1.05±0.01	10.40	1.12±0.01	13.13	1.41±0.02	14.01	1.31±0.01
C					11.13	1.42±0.01			14.37	1.31±0.02
F	7.01	1.54±0.03	8.77	1.69±0.02	10.40	1.74±0.02	13.13	1.76±0.03	13.97	1.76±0.02
F					11.13	1.71±0.03			14.31	1.71±0.04
Mg	7.17	1.70±0.03	8.54	1.73±0.02	10.46	1.64±0.02	12.70	1.67±0.02	14.07	1.79±0.02
Al	7.01	1.99±0.02	8.68	1.79±0.02	10.46	1.69±0.01	12.70	1.77±0.02	13.97	1.75±0.02
Al									14.39	1.76±0.02
Ti	7.01	3.25±0.04	8.68	2.97±0.03	11.18	2.62±0.03	12.70	2.48±0.03	13.97	2.35±0.02
Ti							13.13	2.44±0.03		
Cr	7.05	3.50±0.04	8.69	3.12±0.03	11.18	2.75±0.03	12.30	2.63±0.03	14.25	2.42±0.02
Fe	7.05	3.62±0.04	8.70	3.29±0.04	10.22	3.12±0.03	12.30	2.83±0.03	14.50	2.54±0.03
Ni	7.05	3.68±0.04	8.70	3.43±0.03	10.22	3.27±0.03	12.30	2.96±0.03	14.48	2.70±0.03
Cu	6.83	3.83±0.04	8.62	3.64±0.03	10.36	3.46±0.02	12.27	3.19±0.04	14.03	2.95±0.02
Cu	7.10	3.83±0.04			11.18	3.35±0.04	12.60	3.12±0.03		
Zn	7.05	3.91±0.03	8.54	3.78±0.04	10.46	3.58±0.03	12.63	3.27±0.03	14.07	3.11±0.03
Ga	...	...	8.68	3.89±0.04	11.17	3.64±0.03	12.67	3.42±0.03	14.50	3.18±0.03
Ge	7.05	4.01±0.04	8.54	3.96±0.04	10.46	3.81±0.03	12.43	3.48±0.04	14.07	3.34±0.03
Zr	7.05	4.19±0.04	8.68	4.30±0.04	10.38	4.32±0.04	12.70	4.15±0.04	14.50	3.93±0.04
Mo	7.09	4.06±0.04	8.61	4.24±0.04	10.22	4.28±0.04	12.43	4.17±0.05	14.50	3.96±0.04
Pd	6.83	4.24±0.04	8.67	4.41±0.04	10.27	4.45±0.04	12.30	4.45±0.04	14.11	4.29±0.05
Pd									14.50	4.26±0.04
Ag	6.83	4.27±0.04	8.57	4.41±0.04	10.40	4.49±0.04	12.43	4.44±0.05	14.11	4.39±0.04
Cd	6.83	4.22±0.06	8.62	4.44±0.04	10.35	4.54±0.04	12.30	4.55±0.05	14.02	4.51±0.04
Cd	7.15	4.33±0.05			11.13	4.59±0.04	12.70	4.52±0.06	14.50	4.41±0.05
Cd							13.13	4.58±0.05		
In	6.83	4.25±0.05	8.68	4.45±0.04	10.38	4.62±0.04	12.43	4.64±0.04	14.11	4.62±0.05
In									14.45	4.56±0.05
Sn	6.83	4.21±0.04	8.60	4.48±0.03	10.35	4.65±0.04	12.70	4.69±0.05	14.03	4.66±0.04
Sn	7.15	4.29±0.04			11.18	4.74±0.05				
Sb	7.01	4.28±0.04	8.68	4.48±0.04	10.36	4.69±0.05	12.30	4.73±0.04	14.37	4.68±0.05
Ta	7.05	5.27±0.11	8.67	5.06±0.10	10.27	5.15±0.10	12.43	5.16±0.10	14.45	5.28±0.11
W	7.05	5.37±0.05	8.67	5.17±0.04	10.25	5.21±0.05	12.30	5.30±0.05	14.25	5.40±0.06
Pt	6.83	5.73±0.08	8.57	5.21±0.05	10.40	5.13±0.05	12.43	5.22±0.07	14.11	5.38±0.04
Au	7.05	5.72±0.05	8.66	5.19±0.04	10.40	5.12±0.05	12.43	5.22±0.05	13.97	5.38±0.05
Tl	7.15	5.53±0.05	8.54	5.28±0.05	11.13	5.10±0.05	12.70	5.19±0.06	14.07	5.45±0.06
Pb	7.17	5.86±0.06	8.67	5.38±0.04	10.38	5.21±0.05	12.49	5.22±0.04	14.25	5.42±0.06
Bi	7.01	6.02±0.06	8.67	5.41±0.05	10.38	5.22±0.05	12.49	5.19±0.05	14.37	5.44±0.05
U^{235}	7.05	6.84±0.07	8.67	6.12±0.05	10.74	5.73±0.06	12.67	5.75±0.06	14.25	5.79±0.07
U^{238}	7.05	6.84±0.07	8.67	6.21±0.05	10.74	5.89±0.06	12.67	5.78±0.06	14.25	5.90±0.05
Pu^{239}	7.05	6.83±0.06	8.67	6.32±0.05	10.74	5.88±0.06	12.67	5.82±0.06	14.25	5.83±0.08

primary spectrum. This use of five discriminator scalers on the detector and a similar set, similarly biased, on the monitor provides considerable protection against drifts in bias. The two bias settings permit use, when necessary, of the "window" method of compensation for electronic gain changes (Appendix I).

The deuteron beam energy is determined by differential range measurement at the beginning of a set of runs of a given energy, at the conclusion, and at any time there is an indication that the energy has drifted. The deuteron energy is determined by range in aluminum (to ±1 mg cm^{-2}), which is converted to deuteron energy by Aron's range-energy relation.[15,16] The neutron energy is determined from the kinematics of the $d-d$ reaction, using the energy of the deuteron in the middle of the gas target—i.e., corrections for energy loss in the target foil and in one-half of the target are applied. Fowler and Brolley's tables[17] are used to find the neutron energies. The uncertainty in neutron energy due to uncertainties in range measurement and in the range-energy relation is about 1%. The spread in neutron energy is about ±170 kev at 7 Mev and ±70 kev at 14 Mev, due to gas-target thickness.

The routine procedure consists of alternate open-beam and sample runs. The two open-beam runs preceding and following a sample are combined with the sample run in the computation of the cross section. The background is determined in a similar way with an 18-inch sample of copper, whose direct transmission is less than 10^{-5} at every energy used. Typical open-beam counting rates for the detector are 100 counts/sec.

[15] Aron, Hoffman, and Williams, U. S. Atomic Energy Commission Report AECU-663, second revision (UCRL-121) (1949).
[16] Bichsel, Mozley, and Aron, Phys. Rev. **105**, 1788 (1957).
[17] J. L. Fowler and J. E. Brolley, Revs. Modern Phys. **28**, 103 (1956).

IV. RESULTS

Table I lists the measured cross sections after correction for background, inscattering, and chemical or isotopic composition. The background varied from 1% of the open beam at 14 Mev to 2% at 7 Mev. The inscattering correction was small because of the rather good geometry employed. It was applied on the basis of a formula developed in Appendix II, which was experimentally verified. The inscattering correction is greatest for the heavy elements at the high energies; it increased the uranium cross section at 14 Mev by 0.7% and in most cases was negligible.

The statistical error in the cross sections is typically about 0.5%. Superposed on the counting statistics are other random errors, whose effects make the reproducibility of the data slightly worse than that expected on the basis of statistics alone. These additional errors are most likely caused by short-time changes in gain of the electronic system and by short-time changes in the energy of the deuteron beam. Serious or long-time changes of these types can usually be detected by observing the reproducibility of the ratio of high bias to low bias counts of each counter, which is quite sensitive to these changes, although the two effects can be hard to separate in this way. Some data were discarded on the strength of these studies of high-to-low bias ratios and measured changes in deuteron energy. The over-all error assigned to each cross section has been compounded from reproducibility or statistics (whichever was the larger) plus an arbitrary 0.5%.

Systematic errors in cross section resulting from factors not already considered are difficult to evaluate. Possible sources are voids in castings and contaminants; these have been guarded against by x-ray examination and chemical analysis. Another estimate of systematic error can be derived from the assumption that for the medium and heavy elements the measured cross sections should vary smoothly as functions of neutron energy and of mass number. For the light elements, such as carbon, this assumption is certainly not valid because measurable resonant structure is well known in this energy range. However, for the medium and heavy nuclei, our data are not inconsistent with the assumption of smoothness, even in the neighborhood of magic-number nuclei. For the elements titanium and above, all the experimental cross-section data fit reasonably smooth curves within $\pm 1\%$ when plotted with respect to energy (Fig. 5); and when plotted with respect to atomic number, as in Fig. 6, 80% of the points fit the average smooth curves better than $\pm 2\%$ and 90% fit better than $\pm 3\%$—the worst offenders in the latter case being molybdenum (low by 3 to 5%), and tungsten (high by 1 to 4%).

The agreement at 14 Mev with the data of Coon, Graves, and Barschall[5] is very good, all points agreeing well within experimental error. The agreement with

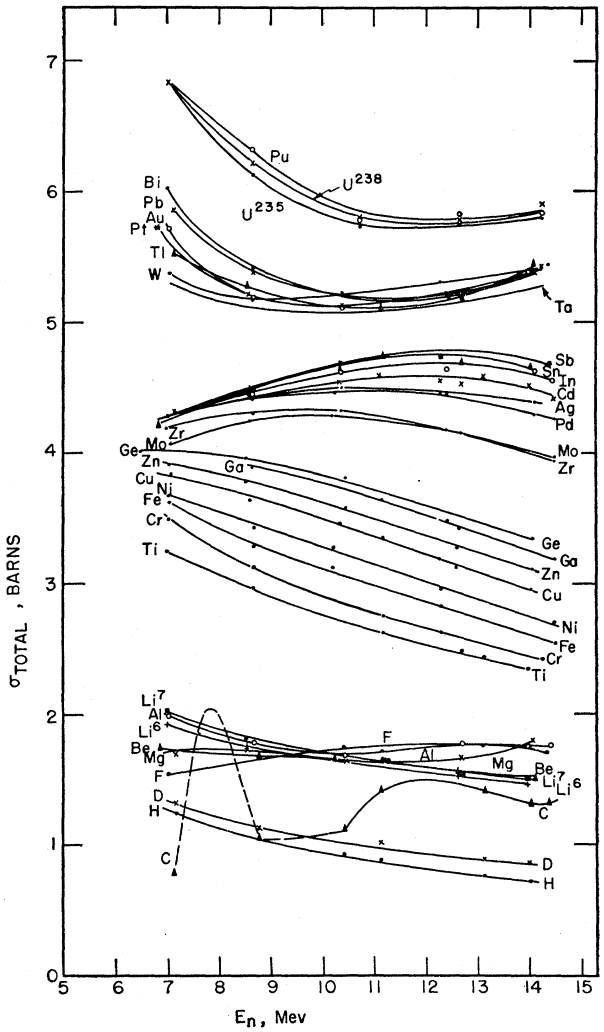

FIG. 5. Contours of total cross section *vs* neutron energy. The lines are smooth curves through the experimental points.

the data of Nereson and Darden[6,7] is in general not as good. For elements up to magnesium our cross sections agree well with those of Nereson and Darden. For elements between aluminum and tin there are a few in good agreement, but typically our cross sections are higher by from 2 to 5%, although the errors overlap. For the heavy elements our cross sections are typically 5 to 10% higher, and the discrepancy seems outside the quoted errors. The disagreement is consistently the worst near 10 Mev.

The smooth curves through the cross-section data are shown together in Fig. 5. These contours of constant mass number form a fairly smooth cross-section surface, which is what is expected on the basis of the optical model.

The experimental data are compared with theoretical predictions of the optical model of Bjorklund and Fernbach[4] in Fig. 6, where the cross sections are plotted

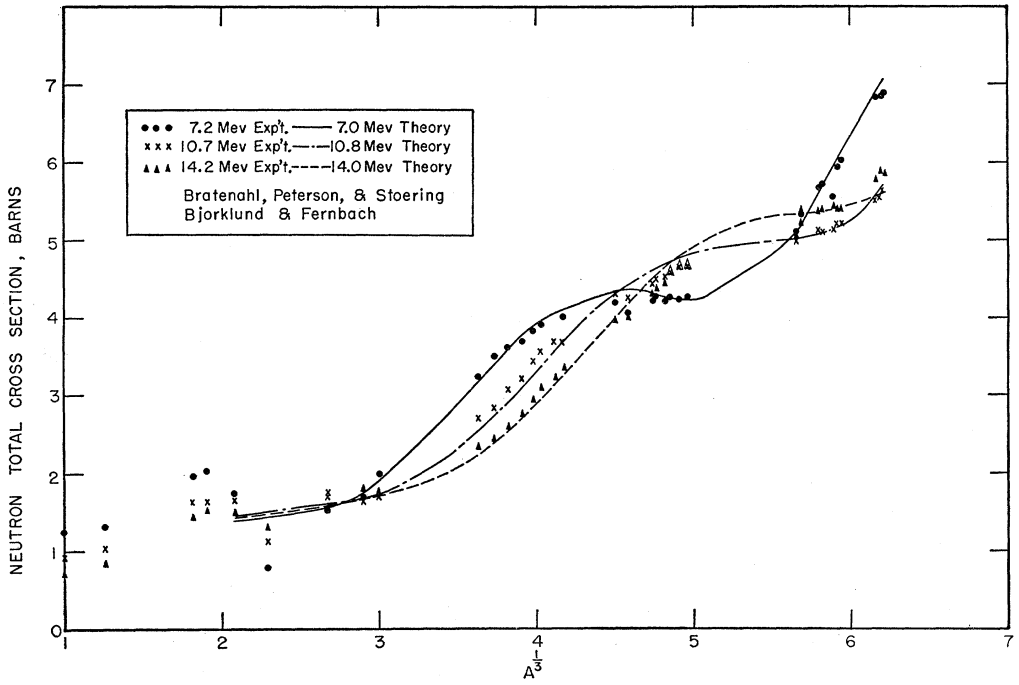

FIG. 6. Comparison of experimental and theoretical total cross sections plotted *vs* $A^{\frac{1}{3}}$ for three neutron energies. The parameters of the optical model of Bjorklund and Fernbach were set by fitting neutron elastic scattering patterns at 7 and 14 Mev.

versus $A^{\frac{1}{3}}$ for three energies. (The neutron energies of the experimental numbers do not quite match those of the corresponding calculations, but this difference is not significant.) The parameters of the model were fixed by fitting the measured elastic-scattering angular distributions at 14 Mev of Gardner, Anderson, Nakada, and

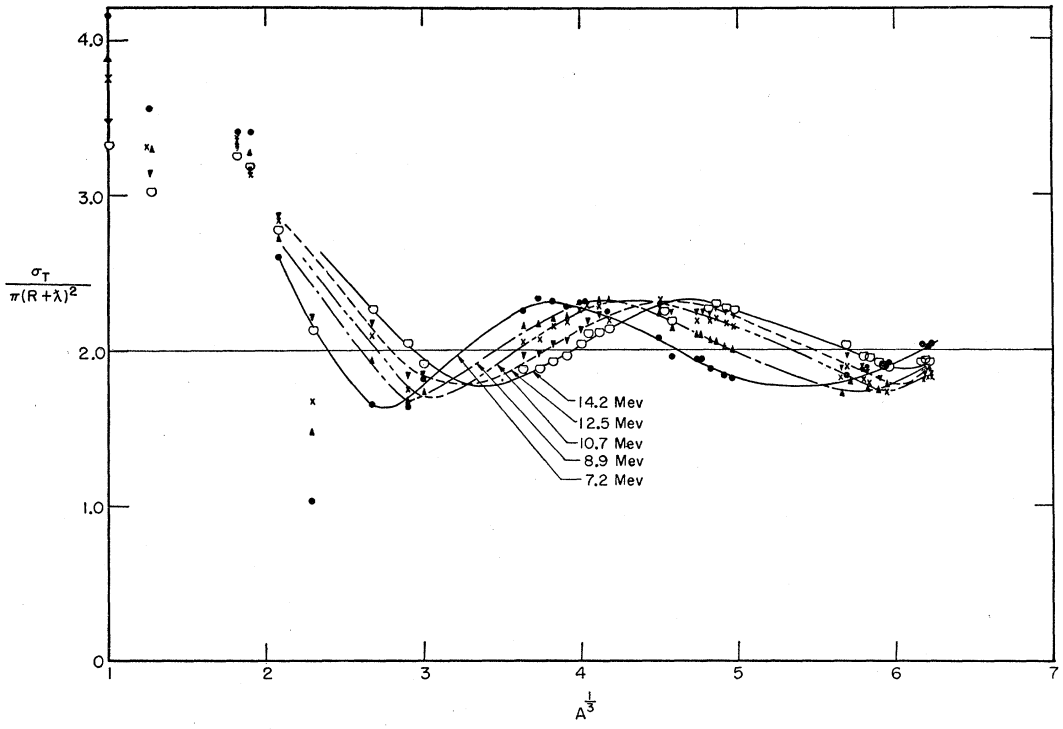

FIG. 7. Plots of experimental total cross sections normalized to $\pi(R+\lambda\!\!\!^{-})^2$ *vs* $A^{\frac{1}{3}}$ for the five energies of measurement. $R=1.4A^{\frac{1}{3}}\times10^{-13}$ cm. These plots emphasize the deviations of the cross sections from the predictions of the "black nucleus" model. The smooth curves are merely averages through the experimental data.

Wong[18] and of Coon *et al.*[19] and at 7 Mev of Beyster *et al.*[20] Figure 6 shows that the total cross sections predicted by this theory fit the experimental points within a few percent for all the elements heavier than magnesium, despite the fact that the curves do not have simple energy and mass dependence.

The deviations of these cross sections from the old, approximate rule, $\sigma_t = 2\pi(R+\lambda\!\!\!^{-})^2$, have some interesting regularities, as is shown in Fig. 7. Here we have plotted the ratio $\sigma_t/\pi(R+\lambda\!\!\!^{-})^2$, where $\lambda\!\!\!^{-}$ is the neutron deBroglie wavelength divided by 2π, and R, the nuclear radius, is taken as $1.4A^{\frac{1}{3}}\times 10^{-13}$ cm. The smooth curve drawn through the experimental points oscillates about the value 2.0 and moves steadily up the nuclear-radius scale as the energy increases.

ACKNOWLEDGMENTS

We wish to thank the many people who helped on this experiment. They include P. Wood, J. Sparks, A. Lorenz, T. P. Stuart, W. Nelson, Barbara Hurlbut, and Marinda Kelley, who helped in running the experiment and data analysis, and O. Tveitmoe, H. Fong, D. Rawles, D. Malone, A. Horn, and D. Telec of the cyclotron crew.

APPENDIX I. BIAS WINDOW METHOD OF COMPENSATION FOR GAIN CHANGES

If one is counting a portion of a spectrum of pulse heights by means of a single pulse-height discriminator (integral bias method), changes in the over-all gain in the detection system (ahead of the discriminator) will change the fraction of pulses of the spectrum which are counted. We shall describe a two-bias method which compensates, to first order, for such gain changes.

Consider a source of pulses whose amplitude spectrum is given by $f(h)$ (pulses per unit pulse height per sec). Let it be normalized:

$$\int_0^\infty f(h)dh = 1.$$

The pulse source is followed by amplification of gain g which transforms the spectrum $f(h)$ into the spectrum $\phi(p)$, where

$$p = gh,$$
$$\phi(p) = f(h)dh/dp = (1/g)f(p/g).$$

An integral discriminator set at pulse height b will have a counting rate given by

$$C_b = \int_b^\infty \phi(p)dp = \int_{b/g}^\infty f(h)dh.$$

The change in count rate C_b due to a change in gain Δg is given by

$$\Delta C_b = (\partial C_b/\partial g)\Delta g = f(b/g)(b/g^2)\Delta g = \phi(b)b\Delta g/g.$$

Now consider a system with two discriminators set at b_1 and b_2, $b_2 > b_1$. We desire to form a quantity which will be independent of small gain changes. Let

$$w \equiv C_{b1} - \alpha C_{b2},$$

where α is a parameter yet to be determined. We require

$$\partial w/\partial g = 0 = (1/g)[b_1\phi(b_1) - \alpha b_2\phi(b_2)].$$

Thus

$$\alpha = b_1\phi(b_1)/b_2\phi(b_2).$$

As a simple example, consider a pulse-height spectrum that has the same amplitude at the bias points b_1 and b_2 (Fig. 8). If b_2 is, say, twice b_1, then α is $\frac{1}{2}$, and the counting rate in the "window" thus formed is

$$w = C_{b1} - \tfrac{1}{2}C_{b2}.$$

If b_2 is near the upper end of the spectrum, we see that the corrective term $\frac{1}{2}C_{b2}$ is small relative to C_{b1}, so that the statistical error in w is not seriously larger than that in C_{b1}.

In our total-cross-section experiment we regularly employed two biases so that this "window" method could be used in reducing the data to eliminate the effect of unknown changes in gain. We observed on a few occasions when gain drifts were suspected that this window method greatly improved the reproducibility of our data. However, by and large, our gain stability was good enough that the window method was not necessary.

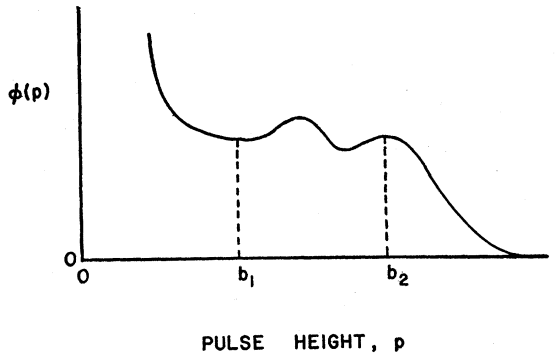

FIG. 8. An example of a pulse-height spectrum.

APPENDIX II. OPTIMUM SAMPLE LENGTH WITH RESPECT TO COUNTING STATISTICS AND INSCATTERING

In choosing the optimum length of a sample for measurement of total cross section by transmission, we consider first the total uncertainty due to counting statistics in the number of detector and monitor counts when counting with the sample in, the sample out, and the long copper bar in the beam (background).

The transmission of the sample is given by

$$T = (d_x - d_B)/(d_0 - d_B),$$

[18] Gardner, Anderson, Nakada, and Wong, Bull. Am. Phys. Soc. Ser. II, 2, 233 (1957); Phys. Rev. (to be published).
[19] Coon, Davis, Felthauser, and Nicodemus, Bull. Am. Phys. Soc. Ser. II, 2, 233 (1957); Phys. Rev. (to be published).
[20] Beyster, Walt, and Salmi, Phys. Rev. **104**, 1319 (1956).

where $d_x=D_x/M_x$, the ratio of detector to monitor counts for measurement with the sample in, and subscripts 0 and B designate "sample out" and "background."

From the cross-section formula

$$\sigma_t=-(1/nl)\ \ln T,$$

where nl is the number of nuclei per cm^2 of beam, we get by differentiation

$$\frac{\Delta\sigma_t}{\sigma_t}=-\frac{1}{n\sigma_t l}\left\{\frac{\Delta d_0}{d_0-d_B}-\frac{\Delta d_x}{d_x-d_B}+\left[\frac{1}{d_x-d_B}-\frac{1}{d_0-d_B}\right]\Delta d_B\right\}.$$

Combining statistical errors in the usual way, using $\Delta D_x=\sqrt{D_x}$, etc., and substituting for d_x, we can rewrite this as

$$\left(\frac{\Delta\sigma_t}{\sigma_t}\right)^2=\frac{1}{(n\sigma_t l)^2(1-d_B/d_0)^2}\left\{\frac{1+d_0}{D_0}+\frac{[T+(1-T)d_B/d_0]^2\{1+d_0[T+(1-T)d_B/d_0]\}}{T^2D_x}+\left(\frac{1}{T}-1\right)^2\left(\frac{d_B}{d_0}\right)^2\frac{1+d_B}{D_B}\right\}.$$

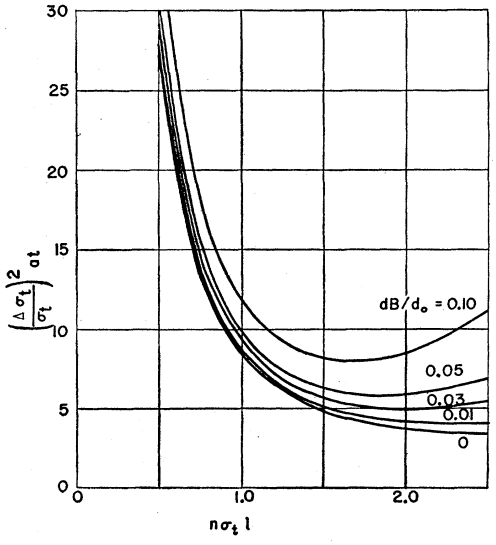

FIG. 9. Square of the relative statistical error times running time *vs* sample length for various background ratios. The curves are computed for sample-in, sample-out, and background counting times to be in the ratio 7:2:1.

Let a be the detector count rate with the sample out, t the total counting time per sample, α the fraction of time for counting with sample out, β the fraction with sample in, and γ the fraction for background. If one alternates sample-in and sample-out, one has the sum of two successive sample-out counts for D_0; if, furthermore, we count background once for, say, every ten samples, D_B is effectively the sum of 10 background counts, each counted for the time γt. Thus we can write

$$D_0=2\alpha at,$$

$$D_x=\frac{d_x}{d_0}\beta at=\left(T+(1-T)\frac{d_B}{d_0}\right)\beta at,$$

$$D_B=10(d_B/d_0)\gamma at,$$

$$\alpha+\beta+\gamma\equiv 1,$$

and the error formula can be written as

$$\left(\frac{\Delta\sigma_t}{\sigma_t}\right)^2 at=\frac{1}{(n\sigma_t l)^2(1-d_B/d_0)^2}\left\{\frac{1+d_0}{2\alpha}+\frac{[T+(1-T)d_B/d_0]\{1+d_0[T+(1-T)d_B/d_0]\}}{T^2\beta}+\left(\frac{1}{T}-1\right)^2\frac{d_B}{d_0}\frac{1+d_B}{10\gamma}\right\}.$$

The problem now is to minimize the quantity $(\Delta\sigma_t/\sigma_t)^2at$ with respect to the four parameters $n\sigma_t l$, α, β, and γ for various conditions of background d_B/d_0 and detector-to-monitor ratio d_0. The resulting optimum is fairly insensitive to d_0, and in the calculations we let d_0 be 0.5, which is typical of our experimental conditions. We found the optimum parameters for various background ratios by first fixing the number of mean free paths $n\sigma_t l$ at 2 (on the basis of rough calculation) and varying a, β, and γ, where $\beta=1-\alpha-\gamma$. This showed for all the background ratios $d_B/d_0=0.01$, 0.03, 0.05, and 0.10 that $(\Delta\sigma_t/\sigma_t)^2at$ was a minimum near $\alpha=0.2$, $\beta=0.7$, and $\gamma=0.1$ and that changing α and γ by 50% from their optima increased $(\Delta\sigma_t/\sigma_t)^2at$ by only 10% or less. Since the error function is so insensitive to the exact values of α, β, and γ (as long as they are approximately optimum), only this one set of optimum α, β, and γ was used in the next step, the calculation of optimum $n\sigma_t l$ for fixed α, β, and γ. The result of this calculation is shown in Fig. 9. The plot shows that the optimum sample length for moderate backgrounds (1 to 5%) is close to 2.0 mean free paths. (We therefore did not reoptimize α, β, and γ.) The ordinate can be read as proportional either to the square of the statistical error for a given running time or to the running time for a

given statistical error. For our background (1 to 2%), a 1-mean-free-path sample would have required twice the running time as our 2-mean-free-path samples, for the same relative statistical error in cross section.

If the background contains a systematic uncertainty, the considerations are somewhat different, of course. In our experiment we felt that the systematic uncertainties in background were relatively unimportant.

Our conclusions on optimum sample length and relative counting times are very close to the results of Rose and Shapiro[21]; their analysis, however, differed from ours in that it did not include any statistical error due to a monitor and did not lump together counts from more than one run for the counts D_0 and D_B.

Another factor that can influence the choice of sample length is the inscattering effect, i.e., the increase in detector counts due to those neutrons which have scattered elastically one or more times in the sample and are then counted in the detector. Following the method of McMillan and Sewell,[22] we write the intensity of neutrons striking the detector after having made just n elastic collisions ($n=0, 1, 2, \cdots$) as

$$I_0=\left(\frac{K}{R_D^2}\right)e^{-l/\lambda},$$

$$I_1=K\left(\frac{A}{R_s^2L^2}\right)e^{-l/\lambda}\left(\frac{\alpha l}{\lambda}\right)\left(\frac{\sigma(0)}{\sigma_{el}}\right),$$

$$I_2=K\left(\frac{A}{R_s^2L^2}\right)\left(\frac{e^{-l/\lambda}}{2}\right)\left(\frac{\alpha l}{\lambda}\right)^2\left(\frac{\sigma(0)}{2\sigma_{el}}\right);$$

in general,

$$I_n=K\frac{A}{R_s^2L^2}P_nf_n \quad (\text{for } n=1, 2, \cdots),$$

where

$$P_n=e^{-l/\lambda}\left(\frac{\alpha l}{\lambda}\right)^n\frac{1}{n!}, \quad f_n=\frac{\sigma(0)}{n\sigma_{el}}.$$

R_D and R_s are the distances of the detector and the sample, respectively, from the neutron source (see Fig. 1), L the sample-to-detector distance, A the cross-sectional area of the sample, l the sample length (which is small relative to R_D, R_s, and L), λ the total mean free path, $\sigma(0)$ the elastic scattering cross section per steradian at 0°, σ_{el} the integrated elastic scattering cross section, α the ratio of elastic to total cross sections (and is on the order of $\frac{1}{2}$), and K is some constant. P_n is the probability that a neutron will traverse the sample and make just n elastic collisions; this expression assumes that the elastic scattering pattern is peaked sufficiently forward that the paths of the scattered neutrons remain reasonably parallel to the beam axis. This assumption is a reasonable one for our geometry and neutron energies and, furthermore, is conservative in the sense that it slightly overestimates the inscattered contributions. f_n is the fraction of n-times-scattered neutrons per steradian at zero degrees to the beam axis. Since the width of the elastic pattern increases about as $n^{\frac{1}{2}}$, the central intensity must decrease approximately as n^{-1}.

The fraction by which the transmitted beam is systematically increased by this inscattering effect is given by

$$\frac{\Delta T}{T}=\frac{1}{I_0}\sum_{n=1}^{\infty}I_n=\left(\frac{AR_D^2}{L^2R_s^2}\right)\frac{\sigma(0)}{\sigma_{el}}\sum_{n=1}^{\infty}\left[\left(\frac{\alpha l}{\lambda}\right)^n\frac{1}{n!n}\right].$$

The corresponding relative correction to the measured total cross section is

$$\frac{\Delta\sigma_t}{\sigma_t}=\frac{1}{n\sigma_t l}\left(\frac{AR_D^2}{L^2R_s^2}\right)\frac{\sigma(0)}{\alpha\sigma_t}\sum_{n=1}^{\infty}\left(\frac{\alpha l}{\lambda}\right)^n\frac{1}{n!n}$$

$$=\left(\frac{AR_D^2}{L^2R_s^2}\right)\frac{\sigma(0)}{\sigma_t}\left[1+\tfrac{1}{4}\left(\frac{\alpha l}{\lambda}\right)+\frac{1}{18}\left(\frac{\alpha l}{\lambda}\right)^2+\cdots+\frac{1}{n!n}\left(\frac{\alpha l}{\lambda}\right)^{n-1}+\cdots\right].$$

For reasonable sample lengths the series converges rapidly. (For this reason one is not greatly concerned about the crudeness of the approximations involved in the higher order terms.)

Note that the inscattering correction to the measured total cross section is almost independent of the sample length. For example, the correction for a 2-mean-free-path sample is only about 30% larger than for a vanishingly thin sample. Since in our experiments this inscattering correction was only on the order of 1%, we would not have improved matters appreciably by using smaller sample lengths.

Measured values of $\sigma(0)$ and σ_t exist for some elements at a few energies in our range, but for our purposes they are not complete enough. If one takes the theoretical expressions[23] $\sigma(0)=(kR+1)^4/4k^2$ and $\sigma_t=2\pi(R+\lambda\!\!\!^{-})^2$, the ratio $\sigma(0)/\sigma_t$ can be written as $(kR+1)^2/8\pi$. Here R is the nuclear radius, and $\lambda\!\!\!^{-}\equiv 1/k$ is the de Broglie wavelength of the neutron times $1/2\pi$. For R we used $1.4\,A^{\frac{1}{3}}\times 10^{-13}$ cm. This theoretical ratio agrees quite well with several measured values at 7 and 14 Mev, so that we had confidence in applying it to all of our inscattering corrections.

Measured values of $\alpha\equiv\sigma_{el}/\sigma_t$ are close to 0.5 (within $\pm 20\%$) at both 7 and 14 Mev. Since in our typical situation a 20% change in α causes only a 6% change in the inscattering correction, we let α be 0.5 in this correction.

[21] M. E. Rose and M. M. Shapiro, Phys. Rev. **74**, 1853 (1948).
[22] E. M. McMillan and D. C. Sewell, U. S. Atomic Energy Commission Report MDDC-1558, 1947 (unpublished).
[23] Feld, Feshbach, Goldberger, Goldstein, and Weisskopf, U. S. Atomic Energy Commission Report NYO-636, 1951 (unpublished).

Putting $R_D=90$ in., $L=30$ in., $R_s=60$ in., $A=0.786$ in.^{2}, and $l/\lambda=2$, we get

$$\left(\frac{\Delta\sigma_t}{\sigma_t}\right)_{\text{inscatter}}=0.26\times10^{-2}\left(\frac{kR+1}{8\pi}\right)^2.$$

To check this experimentally, we placed a detector just outside the neutron cone (and near the normal detector position) and compared its counting rate with and without a 2λ copper sample in the neutron beam. This geometry was slightly, but not importantly, different from the inscattering situation in our transmission experiments. The measured inscattering agreed with the theoretical (modified slightly for the changed geometry) well within the statistics, which were only $\pm40\%$.

PHYSICAL REVIEW VOLUME 110, NUMBER 4 MAY 15, 1958

Possible Analogy between the Excitation Spectra of Nuclei and Those of the Superconducting Metallic State

A. BOHR, B. R. MOTTELSON, AND D. PINES*
Institute for Theoretical Physics, University of Copenhagen, Copenhagen, Denmark, and Nordisk Institut for Teoretisk Atomfysik, Copenhagen, Denmark

(Received January 7, 1958)

The evidence for an energy gap in the intrinsic excitation spectrum of nuclei is reviewed. A possible analogy between this effect and the energy gap observed in the electronic excitation of a superconducting metal is suggested.

THE nuclear structure exhibits many similarities with the electron structure of metals. In both cases, we are dealing with systems of fermions which may be characterized in first approximation in terms of independent particle motion. For instance, the statistical level density, at not too low excitation energies, is expected to resemble that of a Fermi gas. Still, in both systems, important correlations in the particle motion arise from the action of the forces between the particles and, in the metallic case, from the interaction with the lattice vibrations. These correlations decisively influence various specific properties of the system. We here wish to suggest a possible analogy between the correlation effects responsible for the energy gaps found in the excitation spectra of certain types of nuclei and those responsible for the observed energy gaps in superconducting metals.

We first briefly recall the evidence for an energy gap in the spectra of nuclei, and shall especially consider nuclei of spheroidal type. The single-particle level spectra for such nuclei exhibit a particularly close similarity to that of a Fermi gas, since the degeneracies characterizing the particle motion in a spherical potential are largely removed by the distortion in the shape of the nuclear field. The levels remain doubly degenerate, and their average spacing may be most directly obtained from the observed spectra of odd-A nuclei. These exhibit intrinsic states which may be associated with the different orbits of the last particle, and the observed single-particle level spacing is approximately[1]

$$\delta\approx50A^{-1}\text{ Mev},\qquad(1)$$

where A is the number of particles in the nucleus.

If the intrinsic structure could be adequately described in terms of independent particle motion, we would expect, for even-even nuclei, the first intrinsic excitation to have on the average an energy $\frac{1}{2}\delta$, when we take into account the possibility of exciting neutrons as well as protons. Empirically, however, the first intrinsic excitation in heavy nuclei of the even-even type is usually observed at an energy of about 1 Mev (see Fig. 1). The only known examples of intrinsic excitations with appreciably smaller energy are the $K=0-$ bands which occur in special regions of nuclei, and which may possibly represent collective octupole vibrations.[2]

Such an energy gap between the ground-state and first intrinsic excitation indicates an important departure from independent-particle motion, a departure arising from the residual forces between the particles. In lowest order, such forces give rise to a pairing effect, since the attractive interaction is expected to be especially strong for a pair of particles in degenerate orbits. This effect implies a shift upwards, relative to the ground state, of states involving the breaking of a pair. However, to this order, one still expects that levels corresponding to the simultaneous excitation of two particles remaining as a pair will have an average energy spacing of about δ. Such low-lying $K=0$ bands

* National Science Foundation Senior Post-Doctoral Fellow on leave of absence from Princeton University, Princeton, New Jersey, 1957–1958.

[1] B. R. Mottelson and S. G. Nilsson (to be published); F. Bakke (to be published).

[2] See, e.g., K. Alder *et al.*, Revs. Modern Phys. **28**, 432 (1956).